

Darkflight estimates of meteorite fall positions: issues and a case study using the Murrili meteorite fall

M.C. Towner^{1,2}, T. Jansen-Sturgeon², M. Cupak², E.K. Sansom², H.A.R. Devillepoix², P.A. Bland², R.M Howie², J.P. Paxman², G.K. Benedix², B.A.D. Hartig².

Abstract

Fireball networks are used to recover meteorites, with the context of orbits. Observations from these networks cover the bright flight, where the meteoroid is luminescent, but to recover a fallen meteorite, these observations must often be predicted forward in time to the ground to estimate an impact position. This darkflight modelling is deceptively simple, but there is hidden complexity covering the precise interactions between the meteorite and the (usually active) atmosphere. We describe the method and approach used by the Desert Fireball Network, detailing the issues we have addressed, and the impact that factors such as shape, mass and density have on the predicted fall position. We illustrate this with a case study of Murrili meteorite fall that occurred into Lake Eyre-Kati Thanda in 2015. The fall was very well observed from multiple viewpoints, and the trajectory was steep, with a low altitude endpoint, such that the darkflight was relatively short. Murrili is 1.68 kg with a typical ordinary chondrite density, but with a somewhat flattened shape compared to a sphere, such that there are discrepancies between sphere-based predictions and the actual recovery location. It is notable that even in this relatively idealised darkflight scenario, modelling using spherical shaped projectiles resulted in a significant distance between predicted fall position and recovered meteorite.

¹ Corresponding author

² Space Science and Technology Centre, Curtin University, GPO Box U1987, Perth, WA 6845, Australia

1 INTRODUCTION

Camera networks are used to observe fireballs, for the study of meteoroid orbits, and the recovery of meteorites with known orbits. By recording the arrival of a fireball one can calculate the arrival trajectory and hence the orbit and origin within the solar system. If the fireball is large enough that a meteorite falls, recovery of this is often a high scientific priority, as it represents a fresh solar system sample with a known origin. Several networks have been deployed historically, beginning with the Harvard photographic meteor program (Jacchia and Whipple 1956), with the first observed and recovered meteorite being Příbram from the Czech Fireball Network in 1959 (Ceplecha 1961).

Initially these systems were film-based but more recently digital systems have become predominant (for example, (Spurný et al. 2006; Colas et al. 2014; Howie et al. 2017)). The practical techniques they operate upon is to observe fireballs from multiple viewpoints, and then triangulate these bright observations to derive a trajectory in the atmosphere (Ceplecha 1987; Borovicka 1990), and hence backtrack to calculate a heliocentric orbit. In the case of a putative meteorite, for recovery, one uses this bright flight trajectory to calculate forward in time to give a predicted fall position on the ground; the so-called darkflight analysis, allowing ground searches to then be carried out. The details of this darkflight calculation are not often discussed in the literature, except in passing that usually imply that integration calculations were carried out. The calculation is done using the classical drag equation (Equation 1), but this simplicity hides more complex factors. For the starting conditions, what is the shape, mass, density of the meteorite? How do these properties reflect in factors like the drag coefficient? What is the behaviour of the atmosphere at that time and position? How are uncertainties propagated? Typically, bright flight end points are 20-30 km altitude, so there is significant height and time that must be integrated through to get to the ground, and small errors can accumulate resulting in significant errors in the predicted fall position compared to actual landing site. This darkflight calculation is also difficult to verify. By the very nature of darkflight, there are no observations to cross check during descent, so the only criteria for successful modelling is location and characteristics of a recovered meteorite, and a failure to recover may be caused by factors unrelated to the darkflight.

1.1 Historical review

In literature concerning meteorite recoveries, the precise method used for darkflight prediction is discussed, but rarely in full detail. One early example given in (Ceplecha 1961), describing the Příbram meteorite fall, where the winds were a special case of directly against the azimuth of meteor trajectory, simplifying calculations. This predates the widespread use of computers, so calculations were integrated numerically by hand, which the authors describe as ‘laborious’.

Integration steps were every 100 m altitude, and drag coefficient was a function of Mach number, but fixed in subsonic regime to a spherical value of 0.52.

(Ceplecha 1987) (see also (Ceplecha et al. 1998) p390) described their approach in some detail, following the discussion of triangulation methods, as an integration under atmospheric interactions and gravity. They used a Runge-Kutta integrator with a fixed integration step of 10 m (so in space rather than in time) and assumed that after the apparent end of the luminous phase, ablation has ceased and there is no fragmentation, such that meteorite shape does not change. Nearest observational data was used for atmospheric density and wind values, supplemented by a standard atmosphere model (CIRA 1972) if observations were incomplete. Drag coefficient was a function of Mach number (unspecified), with a scalar modifier for a non-spherical nature fixed by using the deceleration at the end point of bright flight. This scalar parameter is in contrast to their work focused on bright flight (Pecina and Ceplecha 1983; Ceplecha et al. 2000) where photometric mass is introduced and used to separate mass from a shape density scalar.

Further publications on notable recovered meteorites briefly mention details of their approaches to darkflight: For the Lost City meteorite, (McCrosky et al. 1971) carry out a numerical integration assuming a spherical rock, using a standard atmosphere, with a fixed drag coefficient of a sphere of 0.92 (using a different nomenclature to 0.52 number for (Ceplecha 1961)). For the Innisfree meteorite recovery, (Halliday et al. 1978) note that they use atmospheric data from the nearest balloon flight observations at Edmonton. (Gritsevich et al. 2014) describe the Annama meteorite observations and recovery, with a Monte Carlo simulation of the darkflight using wind data provided by the Finnish Meteorological Institute. They describe their method in some detail, and begin by fitting the later part of the observed bright flight, calculating forwards and requiring any fragments to have an appropriate shape/density/mass to fit subsequent bright flight observations. For the Desert Fireball Network (DFN) recovery of Bunburra Rockhole (Spurný et al. 2012), the paper summarises the DFN approach as applied at the time briefly, here we describe the current DFN approach in more detail.

Some studies have also focused on the drag coefficient parameter; (Zhdan et al. 2007) describe the drag coefficient of various meteorite shapes, as does (Carter 2011). Additionally, there are many studies on the general aerodynamic drag coefficients for hyper/super/subsonic objects, that we refer to in later sections.

2 METHOD

Here we describe the darkflight modelling technique used by the Desert Fireball Network, discussing the details of some factors that affect the predictions. We illustrate this with case study of the Murrili fireball.

2.1 Overview

The DFN data pipeline is almost completely automated, so it would be in principle possible to generate WRF and darkflight predictions for all triangulations seen. However, such an approach would overwhelm, without some method of filtering. Hence, the choices of which fireballs to investigate in detail is based primarily on the a-b criteria from (Gritsevich 2007; Sansom et al. 2019). Further heuristics that are often considered are considerations of the final observed bright velocity and end height.

For darkflight modelling, one starts with the classical aerodynamic drag equation:

$$\underline{F_d} = - \frac{C_d \rho S V_{mag}^2 \underline{v}}{2m}, \quad \text{Equation 1}$$

where $\underline{F_d}$ is the drag force on the body, C_d is the drag coefficient, m is the body mass, S is the body cross-sectional area, \underline{v} is the unit velocity vector relative to the atmosphere (which includes any contribution from wind movement of the atmosphere) with a magnitude of v_{mag} , and ρ is the atmospheric mass density. Gravitational forces must also be calculated and included for a trajectory calculation.

This equation is used computationally; one integrates forward in time, initiating parameters from the last observed bright flight position, consisting of position, velocity vector, meteorite mass and shape. Figure 1 outlines the calculation steps involved. For every position, the appropriate environmental conditions (air pressure, temperature, density (or humidity), wind speed/direction, gravity vector) are either calculated or looked up in data tables. It is then possible to calculate the Knudsen number, the Reynolds number, and hence the drag coefficient throughout the descent of the body (see Table 1). Hence we calculate forces on the body, accelerations, and update position and velocity vectors using Newtonian mechanics, and account for any ablation effects that will change the mass and hence cross-sectional area, using a theoretical estimation (since there are no observations). For starting conditions, one can also include derived parameters from theoretical modelling of the bright flight behaviour: mass, meteorite shape, and plausible density. One can also impose further conditions that the transition from bright to dark flight must be smooth; most importantly this means that the rate of change of acceleration should be smooth from bright to dark flight (c.f. (Ceplecha 1987)). The DFN approach for the core procedure is monotonic; we assume shape does not change during descent, and that there is no fragmentation (c.f. (Vinnikov et al. 2016)). In reality, it is

quite possible for fragmentation to occur during the darkflight, as seen in meteorites recovered with broken or missing fusion crust (Folinsbee and Bayrock 1961; Spurný et al. 2012). Only a small amount of ablation is predicted between the time after the meteorite ceases to be observed and the time where the velocity has dropped sufficiently for ablation to actually cease, and we implement this in code using the approximation of (Passey and Melosh 1980) equation 2. Typical values for this later ablation are predicted to be <1% of the final mass, which is a relatively small uncertainty compared to other factors.

In common with previously described methods for darkflight integration, the core of the DFN approach is a time series integration. We have tested simple first order time step integration but get slightly better fidelity (in terms of matching fall positions of recovered meteorites) using a 4th order Runge-Kutta integrator.

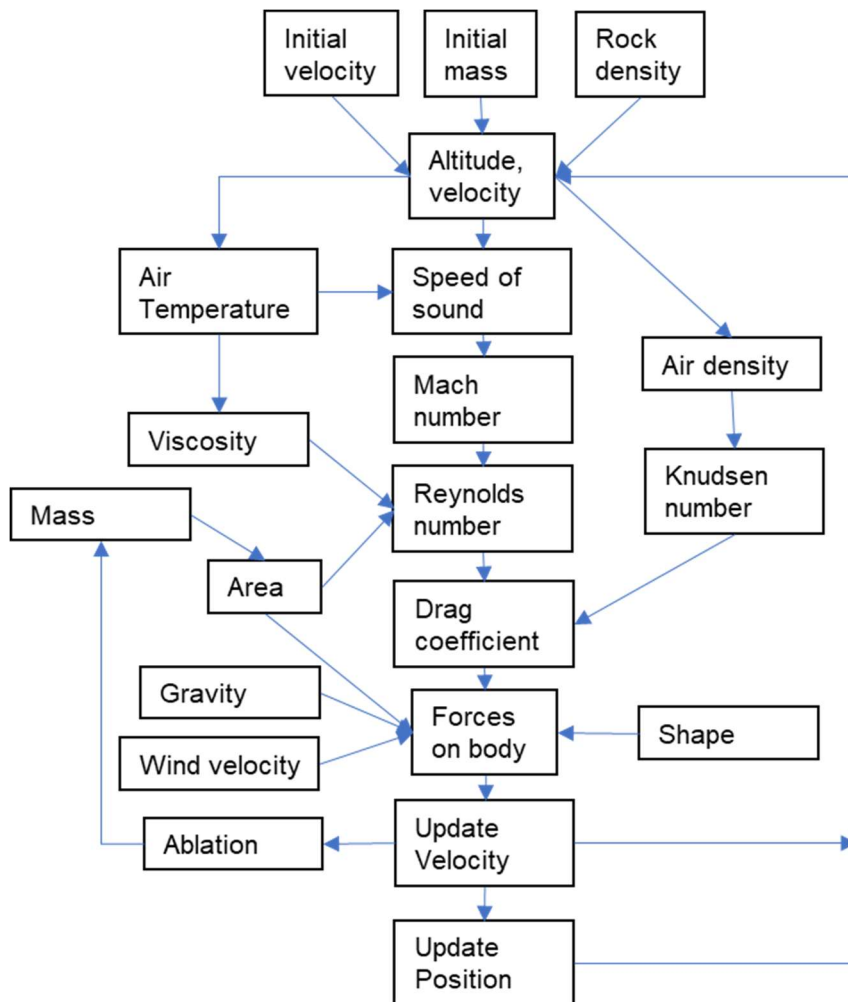


Figure 1 – flow schematic of darkflight modelling.

2.2 Complicating Factors

Darkflight integration presents a unique testing problem, as there are no observations during descent that can offer insight as to the accuracy of the approach. The only ‘test’ available is the recovery—or not—of the meteorite, and its final position with respect to the prediction. To compound this, non-recovery of a meteorite may not indicate errors in darkflight modelling, as it may be a ground searching issue. The only other assistance one may get is serendipitous, non-visual observations; in the case of large meteorite, weather Doppler radar may detect the falling body or bodies (Fries and Fries 2010; Jenniskens et al. 2012), or if a seismic sensor is very close by, the impact may be detected. A specialist instrument such as an active RADAR or LIDAR would assist, but typical ranges are relatively small (few 10s of km) and such instruments are expensive and have not been deployed to date, to the authors knowledge.

From theoretical modelling such as (Sansom et al. 2017) or earlier work such as (ReVelle 2005) and references therein, the shape, density and mass are only partially constrained and are interlinked. However, one can apply some plausible constraints; it is reasonable to expect the density to be close to one of three typical values – approximately 2700 kg/m^3 for an achondrite, 3500 kg/m^3 for a chondrite, or 7500 kg/m^3 for iron (Flynn 2005). Carbonaceous chondrites can have lower bulk densities, in the range approximately 1600-2800 (Consolmagno et al 2006) with a lot of sample to sample variation but are less likely to survive bright flight due to the fragility of that meteorite type and will correspondingly be very rare.

The meteorite shape alone is not usually independently accessible via modelling or observation. The shape may also vary during the bright flight phase due to ablation or fragmentation, although it is commonly assumed to be fixed during darkflight. (An exception is the darkflight modelling of (Vinnikov et al. 2016)). One approach, as taken by (Ceplecha 1987) and similarly used for bright flight modelling (Ceplecha et al. 2000; Revelle 2002; Sansom et al. 2015) is to combine these parameters of shape, density, mass to generate a shape-density parameter (since none of these parameters can be independently constrained from observations), and then use values derived from bright flight as an input to darkflight modelling. This approach in theory forces a smooth transition from bright to dark flight, and in practice becomes an issue of observational errors close to the end of bright flight, which strongly influence the choice of values. The fall position prediction is critically related to the choice of drag coefficient (or shape-density factor) of the meteorite; values too low/high will produce over/undershoot in the fall site prediction. This is particularly a contributor very early in the darkflight, when the meteorite is super- and trans-sonic, and is likely travelling non-vertically, as small changes in the choice of drag coefficient here result in large horizontal shifts in the predicted fall position. Once the meteorite is falling terminally, drag coefficient influences the velocity, and hence the time to fall, and controls the influence of winds. Drag

coefficient is obviously a function of body shape, and this is usually handled as a scalar factor, by giving the meteorite the drag properties of sphere as function of conditions, and then a multiplier to a non-spherical shape (Ceplecha 1987; Zhdan et al. 2007). Shape of course also factors into angle of attack, which will give variation in drag coefficient, and can even produce lift, however the particular orientation of a meteorite in flight is unknown *a priori* so no aerodynamic lift is assumed. Fragmentation can also cause deviation from the fall line by virtue of the fragmentation event adding transverse velocity to the object, deviating the trajectory (for example the Morávka meteorite (Borovička and Kalenda 2003)).

The details of the drag coefficient behaviours chosen do not appear to be discussed in detail in darkflight papers, with the notable exception of detailed modelling such as (Vinnikov et al. 2016). Apart from meteorite properties, drag coefficient is dependent on many conditions; the velocity, the Mach number, the density of air, all of which vary in dark flight as one goes from the supersonic regime in low density air to a subsonic regime in high density turbulent air, close to ground.

The DFN choice of drag coefficient is detailed in Table 1, extending the earlier table in (Sansom et al. 2015) which focused more on bright flight parameters. Values are generated in separate regimes initially: free molecular flow, and continuum regime. For darkflight conditions, the regime is almost always continuum, which is further divided into hyper/supersonic, trans-sonic, and sub-sonic. Darkflight terminal falling is subsonic, which is further divided into turbulent and laminar conditions. The choice of regime is parameterised by Knudsen and Reynolds numbers. (The Knudsen number represents the ratio of molecular mean free path distance to a characteristic dimension.) In all cases related to darkflight, the Knudsen number indicates that calculations are in the continuum regime rather than the free molecular flow regime. The Reynolds number is relatively easy to calculate using the standard formulation, taking the characteristic length as the diameter of meteorite, and when compared to the Mach number, one can choose the appropriate regime to estimate a drag coefficient.

As mentioned, the choice of value of the drag coefficient is critical in the early part of the dark flight, however fortunately for meteorite recovery the hyper and supersonic values of drag are estimated to be relatively simple and only slowly changing over a variety of conditions.

In reality, the choice of drag coefficient is probably an approximation to a complex aerodynamic problem. In darkflight, the meteorite may be tumbling, and ablating slightly early on, and complex shapes can generate lift or transverse forces shifting the trajectory. *Post hoc* estimation of the instantaneous drag coefficients and aerodynamic behaviours using a recovered meteorite shape and appropriate aerodynamic modelling software would make an interesting but complex study, not been done to our knowledge.

1
2

Regime	Value	Symbols and Reference
Free molecular flow Kn > 10	$C_{d_free} = 2 + \frac{\sqrt{1.2}}{2V} \left[1 + \frac{V^2}{16} + 30 \right]$	Kn = Knudsen Number V = velocity, kms-1 (Khanukaeva 2003) equation 3
Hypersonic	$C_{d_hyper} = 0.92$	(For a sphere) (Masson et al. 1960)
Transitional from molecular. flow to continuum 0.01< Kn <10	Bridging function: $C_{d_trans} = C_{d_sub} + (C_{d_free} - C_{d_sub})e^{(-0.001*Re^2)}$	Re = Reynolds number (Khanukaeva 2003) equation 6
Within continuum regime 0.3< M <2.0	Numerical interpolation using Re and Mach number to graphs and tables in (Miller and Bailey 1979); "Sphere drag at Mach numbers from 0.3 to 2.0 at Reynolds numbers approaching 10^7 ", normalised to match the boundary conditions of C_{d_trans} and C_{d_sub}	

Where subsonic drag coefficient is	$C_{d_sub} = \frac{24}{Re} [1 + \exp(2.3288 - 6.4581\varphi + 2.4486\varphi^2) Re^{(0.0964+0.5565\varphi)}]$ $+ \frac{Re * \exp(4.905 - 13.8944\varphi + 18.4222\varphi^2 - 10.2599\varphi^3)}{Re + \exp(1.4681 + 12.2584\varphi - 20.7322\varphi^2 + 15.8855\varphi^3)}$	φ = sphericity (Haider and Levenspiel 1989) equation 11
---	--	---

Table 1 - detailing the regimes and derivations of drag coefficients used in darkflight calculations. We have implemented this as a callable function in Python 3, available at www.github.com/desertfireballnetwork/DFN_darkflight.

2.3 Atmospheric Wind data

During the descent through the stratosphere and troposphere, the atmosphere is not quiescent. Upper atmosphere winds and density variations can deflect the falling meteoroid, such that the ground impact positions may be shifted by several kilometres. In particular, upper atmosphere phenomena such as jet streams are the major drivers of how the fall line is shifted relative to an analysis without considering winds. To predict these atmospheric properties, the DFN uses the NCAR atmospheric modelling system Weather Research and Forecasting (WRF) version 4, with ARW dynamic core. (Skamarock et al. 2019)³. The WRF is a forecast model that incorporates real world data (such as balloon flights) to model atmosphere dynamics, capable for being initialised from a global data set to generate mesoscale results at high spatial resolutions suitable for inputs into a darkflight calculation. The WRF software generates a weather simulation product as a three-dimensional data matrix in a latitude/longitude/height cuboid around the bright flight end point. From the model, grid values are extracted for the atmospheric properties of relevance to darkflight. This includes the pressure, density, temperature, relative humidity, horizontal wind speeds as function of height, latitude, and longitude (in u, v coordinates), such that these can be interpolated during darkflight modelling in 3D to precise locations. Since the WRF data cuboid is not necessarily north-south orientated, wind values must be extracted; this extraction therefore involves a coordinate transform, as WRF grids are not typically aligned with true north, and local verticals may also need to be corrected. For convention in our calculations, we define wind directions in degrees, with North=0, East positive, with a positive wind magnitude in direction of wind travel, not the wind's origin.

The primary use of the WRF tool is weather forecasting. The top level forecast is done on a global matrix - extrapolating the state of the weather matrix, based on past observations using a physical model of the atmosphere, to the future. The global matrix is typically applied with a time step/resolution of 6 hours. This top level product then initialises finer resolution modelling over a smaller area in order to achieve better precision both in time and space. To get detailed (fine grid) forecast for a local area, a set of embedded domains is defined (typically 4 levels), increasing in cell size resolution, to finally achieve typically 1 km resolution around the bright flight end point. Each domain is based on the physical model of the atmosphere, with the boundary states coming from higher level matrix points. However, in the darkflight modelling case, we are not forecasting, but interpolating the past state of weather. We do this along the

³ <https://rda.ucar.edu/datasets/ds083.2/>

meteoroid dark flight trajectory using a physical model of the atmosphere based on the observations rather than forecast, using the archived data from the NCEP FNL Operational Model Global Tropospheric Analysis online datasets⁴. These archived snapshots contain constraints on the global weather conditions at each time step, with a six hour interval. When hindcasting the conditions, one starts with a snapshot, and propagates the weather model forward in time (and at higher spatial resolution in the location of interest). The propagation has forcing conditions, such that the results generated must pass through the conditions recorded by later snapshots, including snapshots of times after the meteorite fall.

Due to the stochastic nature of the WRF numerical modelling software, slightly different results are produced each time it is run, even with the same input data, but the model outputs do not provide any error analysis. Variations arise from floating point precision, and from the limitations of the hardware and numerical libraries used. As its primary purpose is weather forecasting, the success of the modelling is evaluated by comparing the forecast with real weather observations. It is also worth noting that observational data for central Australia is somewhat sparse. To resolve this lack of defined error bars, for each studied case of possible meteorite fall we run models starting from different archived global snapshots, typically 0-6 hours, 6-12 hours and 12-18 hours before the fall time, and then extract from the results the conditions and wind profile at the time of the meteorite fall. Comparison of these multiple cases highlights how stable the weather was, to explore uncertainties in the product introduced by the known errors in the observational data and the ability of the model to work for specific weather situations. For example, a stable weather situation is more likely to give very similar sets of wind profiles, while a cold front passing shortly before the time of the fall can be expected to produce a lot more diversity in the vertical profile plots extracted from the three individual modelling products of the different time windows. The amount of profile variation provides insights as to how to constrain our Monte Carlo darkflight simulations (as described below).

2.4 Implementation details

For the DFN operations, we have implemented a darkflight integrator in Python 3, using the SciPy, NumPy and AstroPy libraries as needed (Jones et al. 2001; Astropy Collaboration et al. 2018). SciPy includes the core Runge-Kutta integrator function. We use the WRF-python library provided by NCAR to access the data files produced by WRF, and several smaller libraries are used for geocentric coordinate transforms. The resulting tool takes as an input the results from a triangulation, plus putative meteorite characteristics, and a data file from a

⁴ DOI: 10.5065/D6M043C6

WRF scenario, and produces time-position trajectories to ground. This tool can then be iterated over to investigate multiple scenarios, to produce likely fall positions for practical use for ground meteorite searching.

This darkflight integration can be carried out in an Earth inertial coordinate system, or in an Earth Centre Fixed frame (where Coriolis force must be included as the atmosphere is coupled to the Earth's rotation on short timescales), A geodetic Earth model is used, and the gravity vector is calculated as perpendicular to the Earth's reference ellipsoid.

The resulting product of darkflight aims to predict a likely search area for a meteorite. The most basic result is a fall line - a ground plot showing a line giving fall positions for a given range of proposed masses. For the DFN, a wide range of masses are modelled, to aid in searching planning; generally this range is much larger than the expected uncertainty of the final mass, which is obtained from bright flight modelling (Sansom et al. 2020). This can be produced for multiple scenarios such as different assumed shapes or wind profiles, resulting in multiple fall lines. In Figure 2 we plot this simple case for the Murrili fall, discussed in more detail in following section. We show two scenarios: idealised spherical and a brick-shaped meteorites. Note the curved shapes of the fall line, and the offset caused by shape choice; the curve is a result of the influence of the atmospheric winds, whereby drag coefficients are generally higher for smaller bodies.

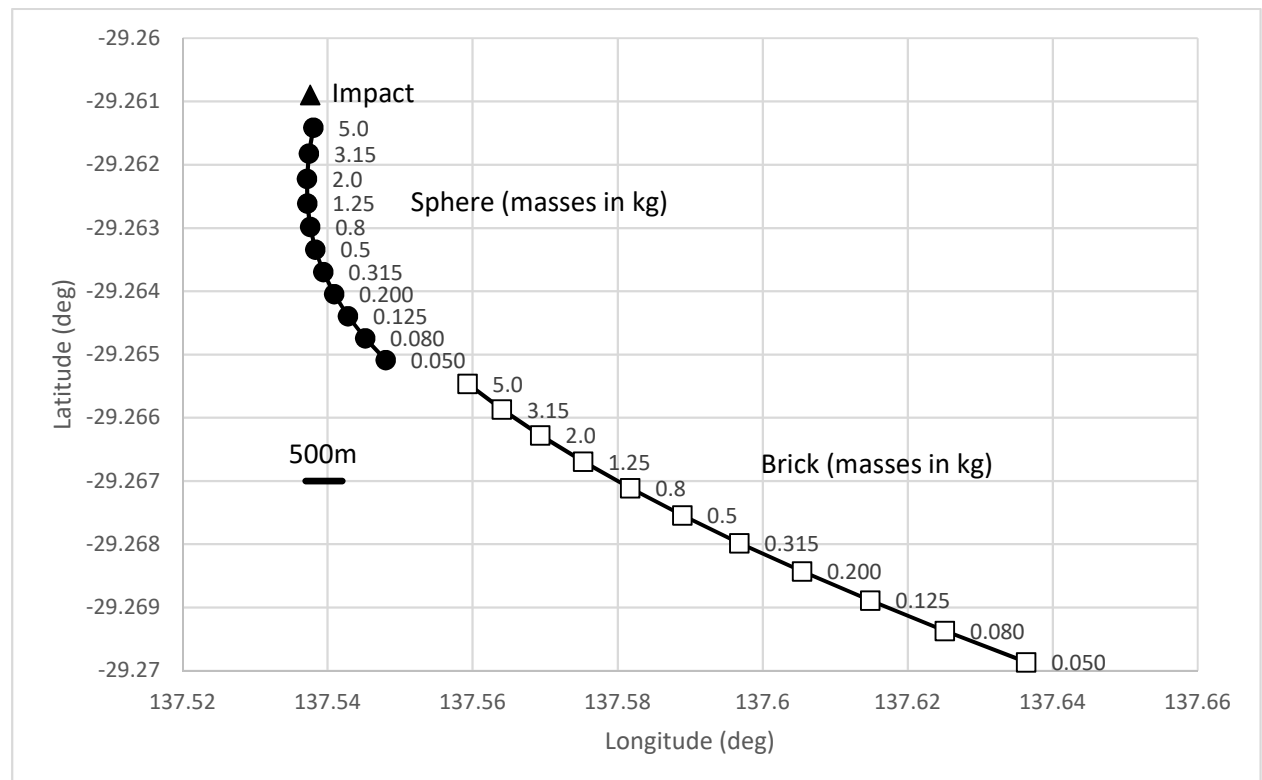


Figure 2 - Fall line predictions from the Murrili bright flight endpoint, assuming a chondritic sphere, and brick, using the wind model 06:00 snapshot as described in the following section. The actual recovered fall position is marked with black triangle.

For searching, of greater use is an impact probability scatter plot or heat map. To generate heat maps, a Monte Carlo approach is used, varying both the meteorite input parameters, and the atmospheric variables. Monte Carlo modelling can be computationally expensive, but as a bare minimum, several scenarios can be calculated since the meteorite shape/density/mass is estimated from modelling (Sansom et al. 2017) but not known with certainty. The dimensions of the Monte Carlo scatter can be used to inform the likely width of the uncertainty in the fall line, which allows searchers to prioritise their activities in the most time-efficient manner. To highlight all the subtleties and complexity involved, we describe in detail the analysis related to the Murrili meteorite fall (Sansom et al. 2020).

3 MURRILI METEORITE FALL AS A CASE STUDY, WITH DISCUSSION

The Murrili fireball provides an interesting case study of the effects and importance of detailed modelling of the darkflight. The fireball that resulted in the Murrili meteorite occurred over Kati-Thanda (Lake Eyre south), in South Australia at 2015-11-27T10:43:45.5 UTC. The fireball was observed by the DFN, and the meteorite recovered within the following month. Hence the recovered shape, density, and mass can be used to back validate darkflight modelling. Murrili is a fortunate case as the scenario was quite ideal from the point of meteorite recovery (although the ground conditions were difficult): The fireball had a well observed bright flight, almost equidistant between four DFN all sky cameras, that all captured the full event with high quality data (Wilpoorina, William Creek, Nilpena and Etadunna), supported by two more distant cameras at Billa Kalina and Mount Barry that also contributed. The trajectory was relatively steep, with a zenith angle of 21.8° , and the fireball penetrated deep into the atmosphere, to a low altitude of 18.0 km. The triangulation, modelling and recovery is described in detail in (Sansom et al. 2020).

The steepness, and the low final altitude dramatically reduce the influence—and hence the associated uncertainties—of the local wind conditions, reducing the errors compared to less favourable examples, such as a shallow entry angle with an end point altitudes that could be much higher (over 30 km in some cases). This combination of factors makes Murrili a case study where one can investigate the limitations of darkflight modelling – the almost ideal experimental situation should result in predictions that closely match the recovered fall position, provided the model is accurate.

Further confidence for meteorite searching and fall position was given by aerial reconnaissance of the site, using a light aircraft from William Creek (by authors MC and BD), that observed a visible splash in the lakebed, at the area of the expected the meteorite fall. Approximate coordinates from the light aircraft were used to begin ground searching. This single splash also supported the lack of significant fragmentation seen in the bright flight images.

3.1 Constraints from bright flight observations

The factors as mentioned above resulted in a low uncertainty in the end position and velocity, as detailed in Table 2.

Date/time	2015-11-27T10:43:51.626 +/- 0.05
Longitude, degrees East positive	137.47817 +/- 50 m
Latitude, degrees	-29.26534 +/- 50 m
Height above WGS84, m	17960 +/- 40
Velocity, m/s	3280 +/- 210
Zenith angle, degrees (from vertical)	21.80 +/- 0.05
Azimuth angle, degrees (north = 0, clockwise positive)	82.60 +/- 0.05

Table 2 showing the end of bright-flight parameters, used for the initiation of darkflight calculations. See (Sansom et al. 2020) for further details.

As discussed in detail in (Sansom et al. 2020), the final mass prediction was for a value of 1.9 kg, +/- 0.4 kg, assuming a chondritic density of 3500 kg/m³. The best fit modelling to the luminous trajectory using first the α - β approach of (Gritsevich 2007; Sansom et al. 2019), and then an Extended Kalman Filter (Sansom et al 2015) was relatively smooth, showing no evidence of major fragmentation, and giving a Shape Change Coefficient which matches well with typical values, so this event does not stand out significantly as indicating an unusual shape, or any strong deviation from expected path (such as might be from lift or strong asymmetry).

Single object (sphere) darkflight integrations

We begin by considering a integration case, and discuss the effects of factors such as wind modelling in the following sections. In Figure 3 we plot the calculated sphere drag coefficient (C_d), and fall velocity as function of altitude. We see that C_d does change significantly during descent, as velocity and atmospheric density both vary, in particular early on when velocity is still dominated by the arrival velocity, rather than terminal effects. Darkflight encompasses the

full supersonic to subsonic regime, and this illustrates the importance of varying C_d . Murrili is almost an ideal case, with short darkflight, this effect would be more pronounced for a meteorite at say a shallow angle, from a higher altitude.

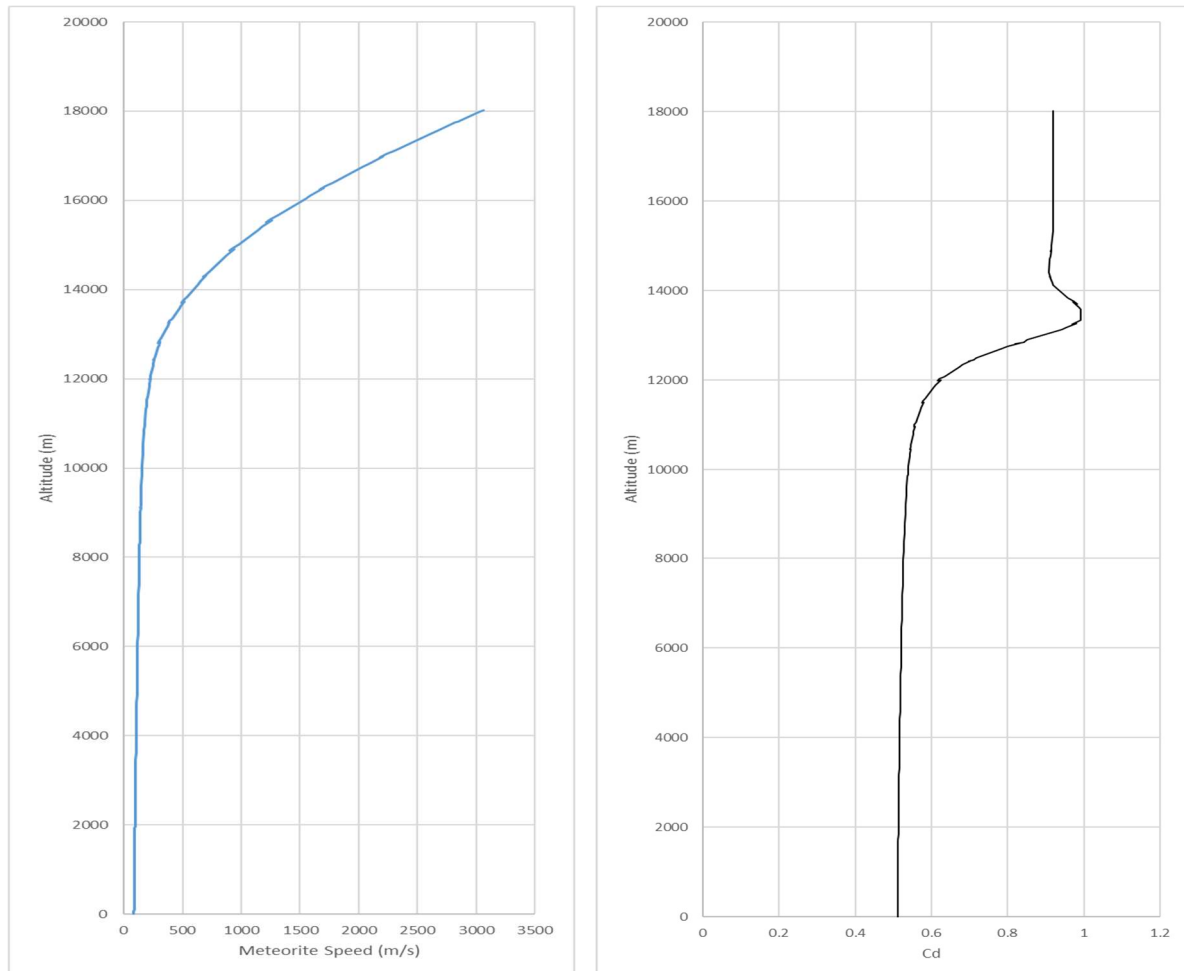


Figure 3, showing modelled Murrili fall speed, and drag coefficient as a function of altitude

In Figure 4 we show the idealised model trajectories viewed from above for several chondritic spherical masses, equivalent to generating the sphere fall line shown in Figure 2. This illustrates the effect of winds on fall position, and how the fall line is constructed. Even in the case of Murrili, with a particularly low end point and steep trajectory, a 1kg sphere is still deviated significantly in predicted fall position compared to a no-wind scenario.

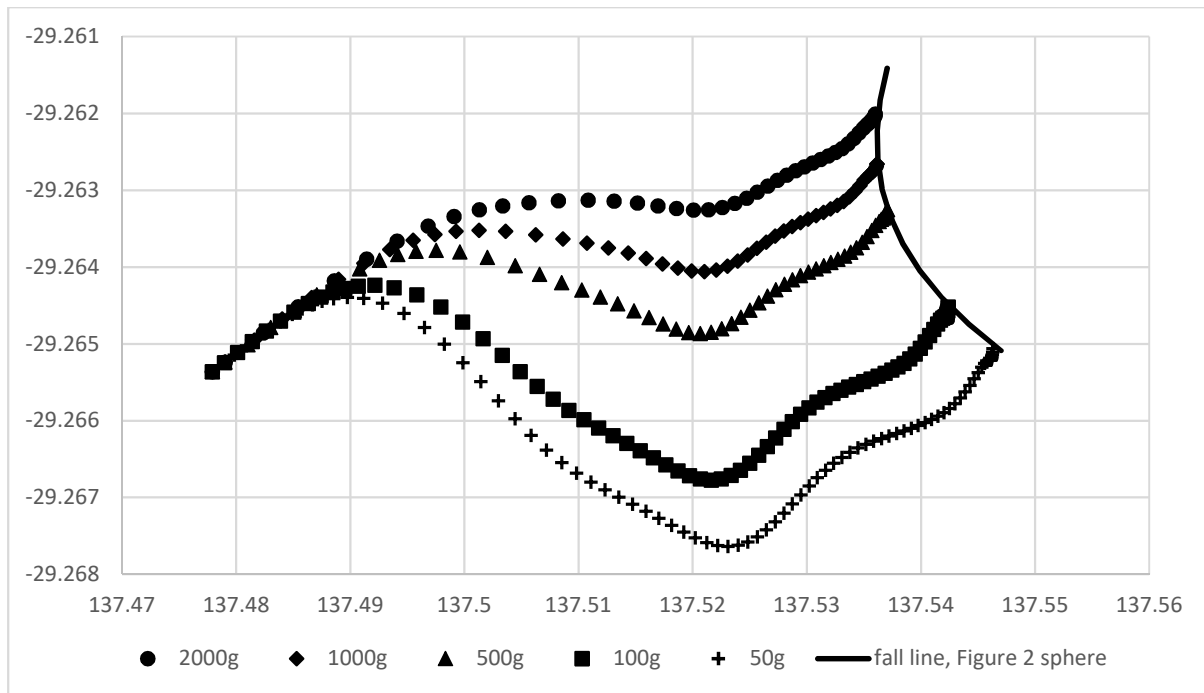


Figure 4 modelled trajectories of chondritic spheres for different masses in longitude and latitude, showing the influence of winds and atmosphere during descent, from Murrili bright flight endpoint.

3.2 Effects of variation in wind profiles on fall lines.

Wind data is generated using the WRF model. In the case of the Murrili meteorite, we used version v3.7.1 for the fall coordinate predictions prior to meteorite searching, and later v3.9.1 as it came available for re-running of the initial analyses (Skamarock et al. 2008).

As is seen in Figure 2 and Figure 4, the atmospheric winds distort and shift the fall line, in a mass dependent manner. However, this wind profile used is a modelling prediction generated by WRF, with no way to be independently directly verified at this locale.

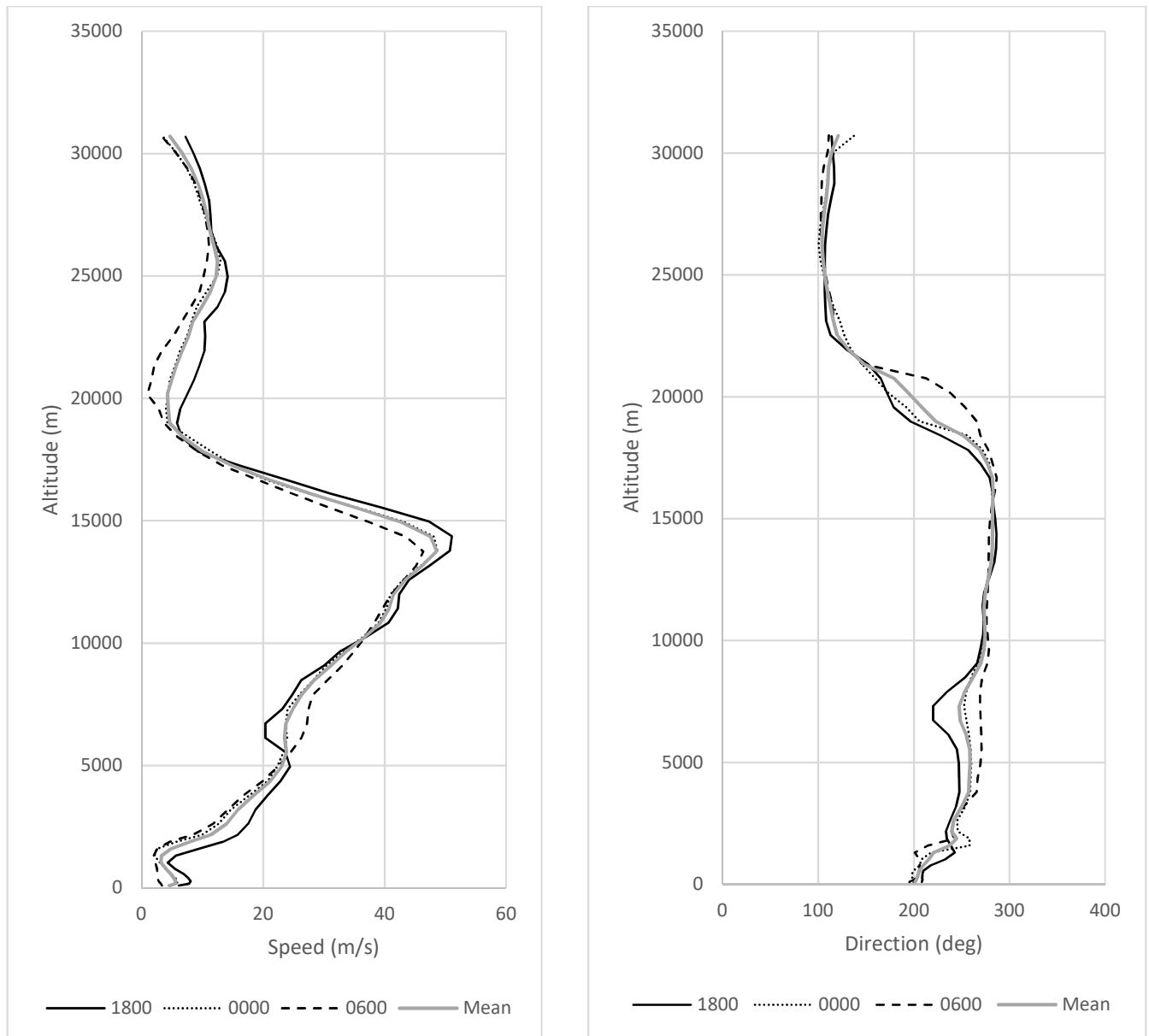


Figure 5 plot of wind profiles from each WRF model run for comparison. Dominating westerly winds at altitudes 10-15km are typical for the subtropical jet stream in the area of the fall. The individual profiles are products of WRF runs starting from the snapshot 2015-11-26 18:00 UTC, 2015-11-27 00:00 UTC and 2015-11-27 06:00 UTC.

As mentioned, WRF can be initiated with archived global snapshots at six hourly intervals. Examination of the spread of profiles from these snapshots is one method to generate an estimate of the plausible variation in wind models to use within any Monte Carlo simulation. In Figure 5 plot of wind profiles from each WRF model run for comparison. Dominating westerly winds at altitudes 10-15km are typical for the subtropical jet stream in the area of the fall. We plot results from three model runs based on different snapshots. Note that the winds are exceptionally strong at the 15,000 m levels, indicating a jet stream effect, and in fact greater

than have been observed in most other cases investigated by DFN. There is also some variation between outputs from each snapshot. Regional historical weather maps for this area of Australia for the 25-30th November 2015 show a high pressure region passing to the south of the fall area, with a change in general wind direction on the 26-28th November. The precise timing of this change may well have taxed the fidelity of WRF to carry out a high spatial-temporal resolution simulation far from actual archived weather observations. One can investigate the gross effect of this wind variation by carrying out darkflight calculation for Murrili for ordinary chondritic-density spheres using the results from each wind model, as shown in Figure 6.

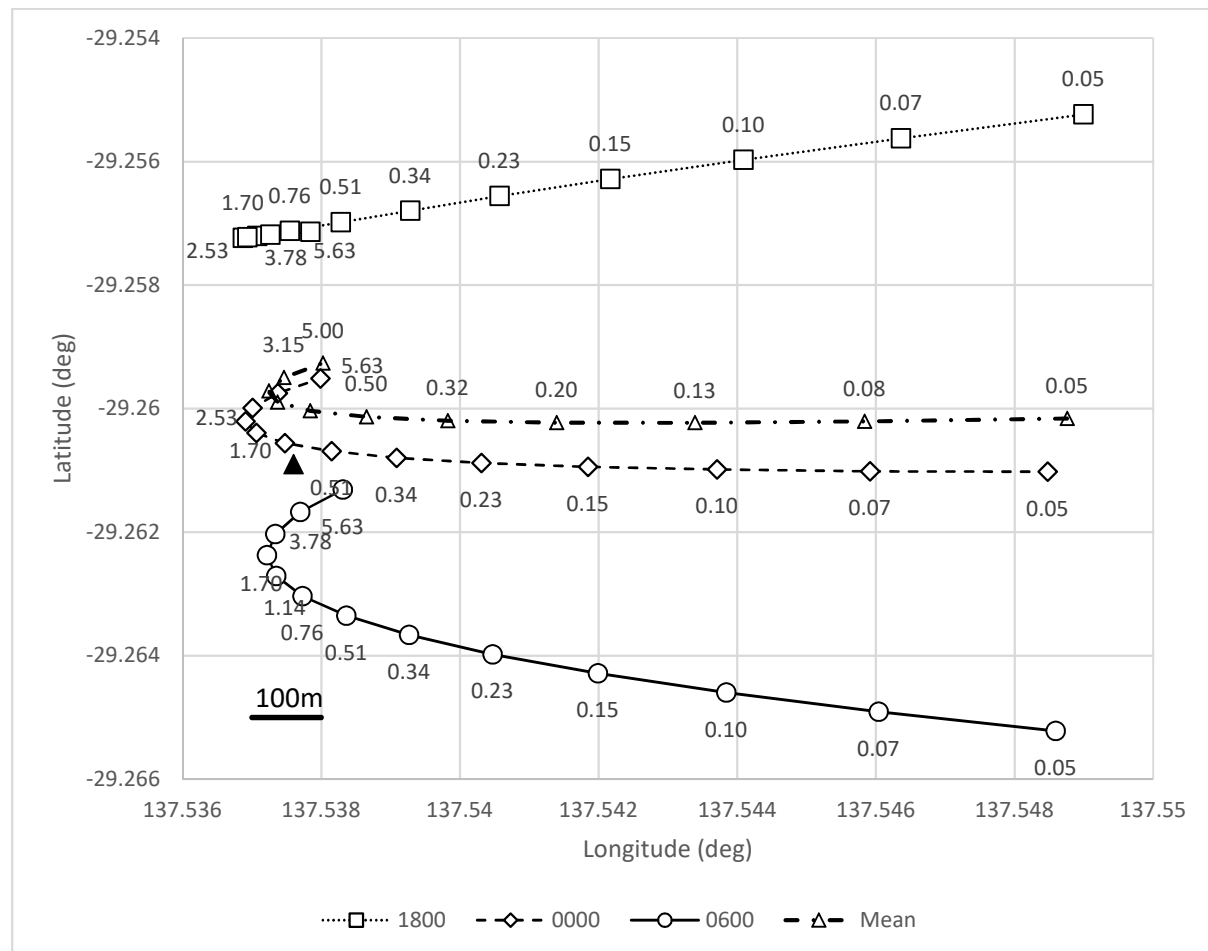


Figure 6 Variation in fall line predictions for chondritic spheres due to variations in WRF wind model data, model snapshot shown in legend. Numbers along line indicate the mass on ground. Some numbers omitted for clarity on some lines, but the points shown correspond to matching mass markers on the lowermost curve. The final recovered meteorite fall position (1.68 kg) is also shown with a solid triangle (▲).

There are significant variations between ground predictions from the wind models, typically 200-300 m between lines. This strong wind dependence is in part a consequence of the structure of the drag equation, where relative velocity is a squared factor (Equation 1). In the

bigger picture of conducting ground searches in the Australian outback, this can be an issue, as accepting such variations produces an unrealistically large search area that is not feasible to search (compounded by the other uncertainties discussed in following sections). Ironically, it appears that although the Murrili triangulation scenario was ideal, darkflight conditions were poor. Of some hope in the case of Murrili is that most plausible mass ranges—from bright flight estimates (Sansom et al. 2020)—are close to the western edge of the fall lines, at the areas of most fall line curvature. So in this case, this means that the area that needed to be searched was relatively constrained, regardless of the choice of wind models.

More generally when wind model scenarios diverge, at one extreme one can elect to search all areas, or one can prioritise. For this and previous searches, when faced with this choice, the DFN has usually elected to focus on the penultimate/2nd-shortest WRF model outputs; in this case starting from the snapshot from 2015-11-27 00:00 UTC. This is purely an empirical choice, based on backwards comparison of almost all of the DFN recovered meteorites (and with hindsight a good match to Murrili as well) (Spurný et al. 2012; Spurny et al. 2012; Sansom et al. 2020). This may be a result of the mechanics within WRF that implies that longer runs are needed for accuracy, to allow the WRF model to achieve numerical stability, whereas the longest simulations allow deviations from reality to accumulate. We lack the expertise in climate modelling to comment in detail, and this is clearly an area that needs further study and more data, as very few meteorites exist with both known precise end points, and well characterised, published, detailed shapes and densities. As such, our approach is to empirically use the penultimate wind model, ensuring that searching in the field is aware of the limitations of this approach. It is worth noting that it appears that Murrili is a particularly variable WRF scenario; in previous DFN searches the fall lines from different WRF snapshots are often closely overlapping, such that it is possible to search all scenarios within a reasonable timeframe and a judgment on choice of wind profile is not required. In this case, it was fortunate that the fall was on a salt lake, allowing the use of quadbikes to search large areas relatively quickly in comparison to foot searching in a vegetated area.

However, wind is not the only uncertainty affecting fall position in darkflight calculations; one must also consider shape and meteorite density, which can be partially constrained but is effectively unknown.

3.3 Effects of shape and density

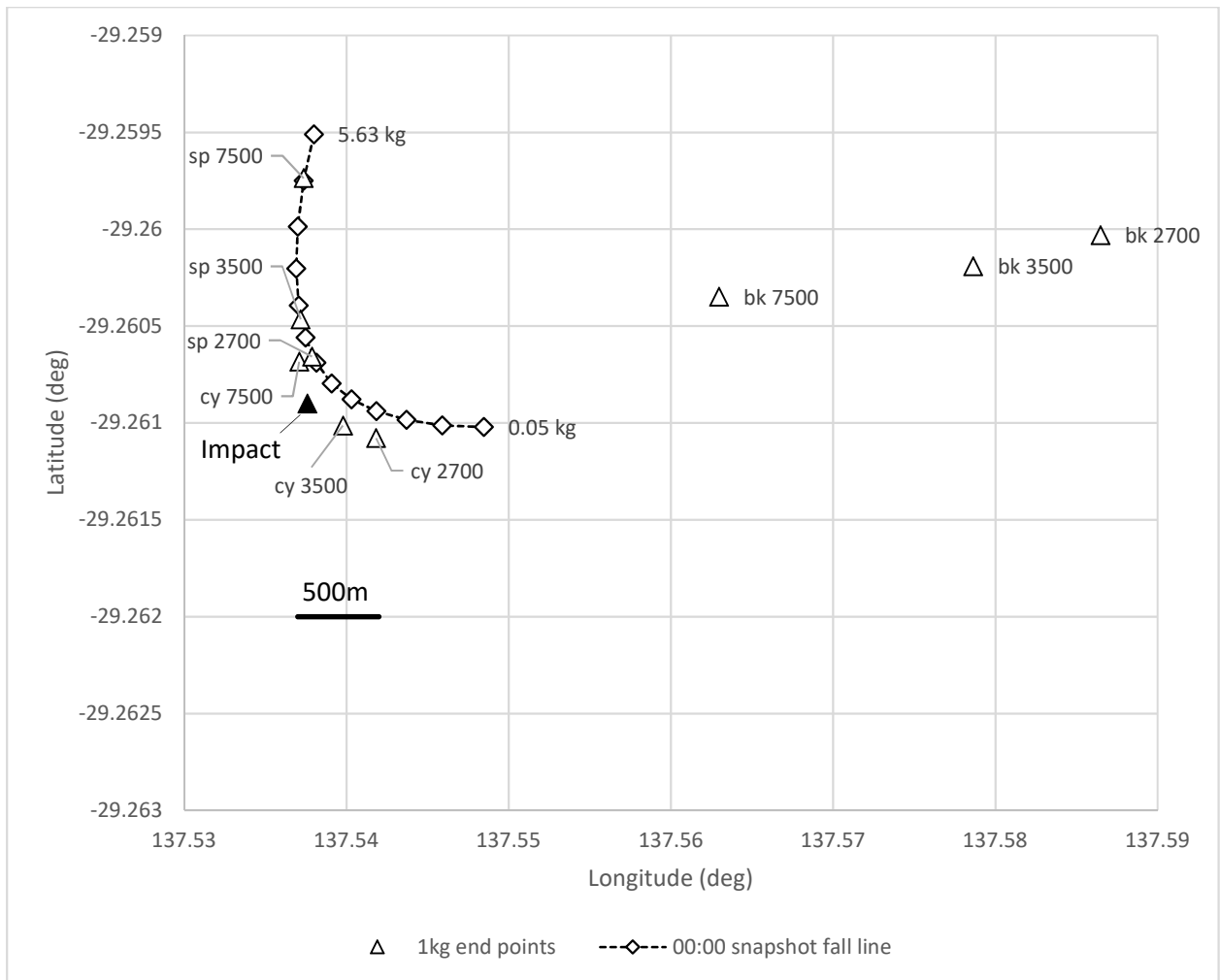


Figure 7 plot showing the effects of density and shape on final position of a hypothetical 1kg object. Shapes plotted are sphere, cylinder, and brick (as defined in the text). Density of the object is constrained to 2700, 3500, and 7500 kgm^{-3} . For comparison we include the fall line based on the 2015-11-27 00:00 UTC wind snapshot (3500 kgm^{-3} sphere, varying mass) and the impact point from Figure 4

To investigate the effect of meteorite shape and density choices on predictions, Figure 7 plots darkflight predictions for three different densities (2700, 3500, 7500 kg/m^3), and three different shapes (sphere, cylinder and brick, as defined by (Zhdan et al. 2007), compared to the 00:00 snapshot fall line. The change in shape (which effectively changes drag coefficient) and density (which changes cross sectional area for the same mass), have direct effects on the fall line position, and in this case (and in other cases seen by the DFN (Devillepoix et al. 2018)), choice of shape has a greater influence than meteorite mass or density prediction. For density variations, this results in same mass falling on effectively the same fall line but translated along the line. This is also the case when changing shape from cylinder to brick, however this shift is more extreme. From the DFN experience of recovered meteorites a 2.5 x 1.5 x 1 brick shape will be an outlier; in general, recovered samples seem to be best fit by

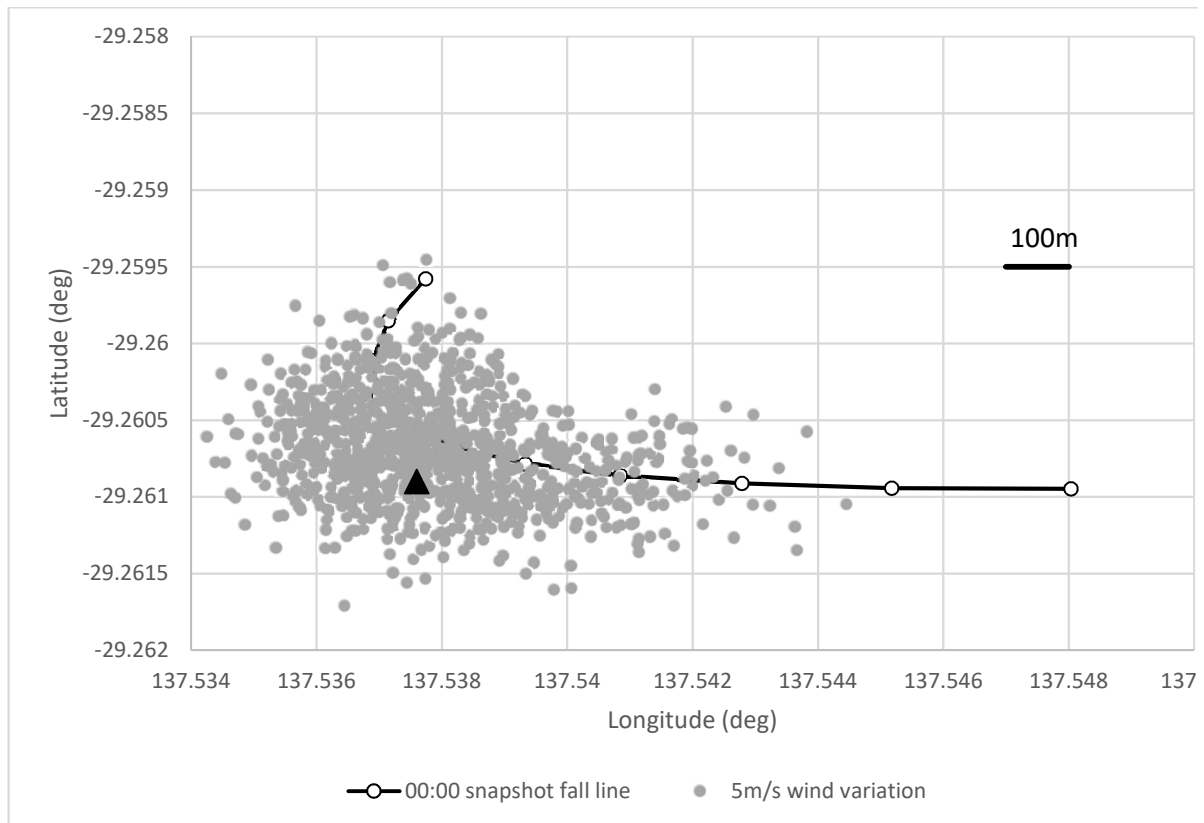
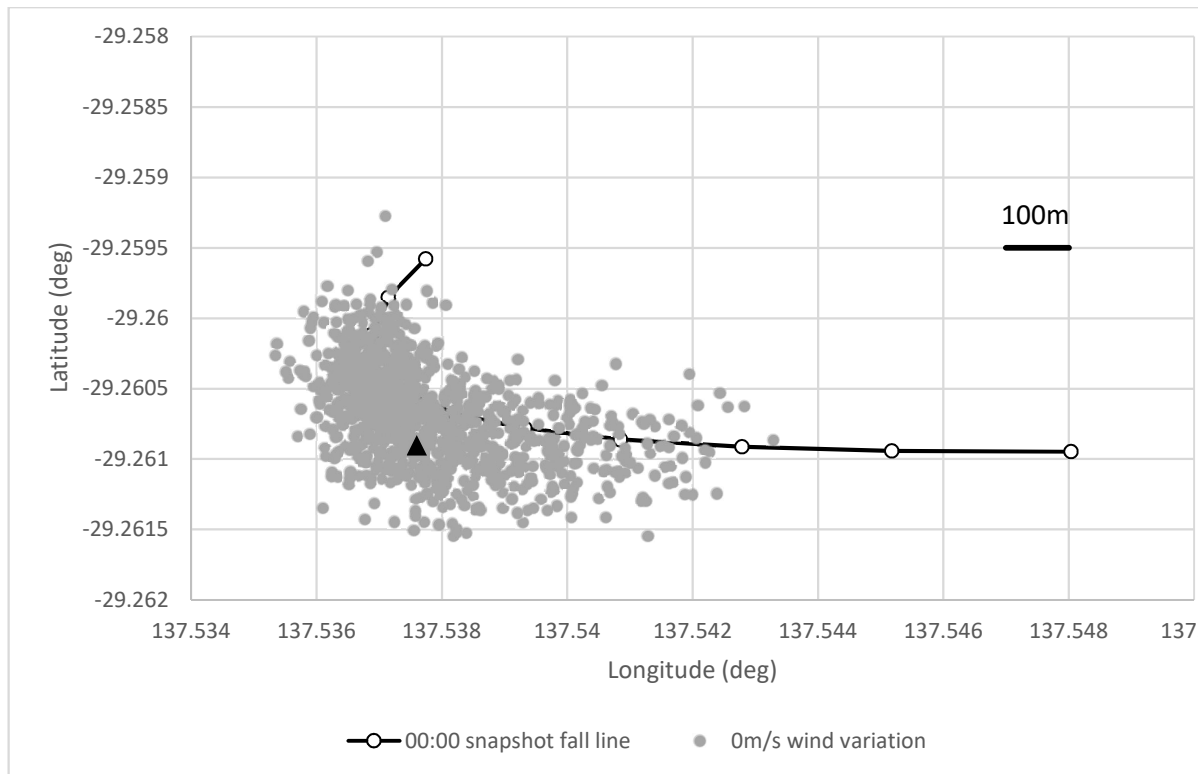
drag coefficients close to spherical. Furthermore, it is worth noting the dominance of shape choice: effective drag coefficient is changed by a factor of 1 to 2 (Zhdan et al. 2007), and although density effects are varying comparably (through the cross-sectional area), the shape effects dominate. This effective along-line shifting effect has advantages and disadvantages for searching. Traverse distance from the line that must be searched is essentially unchanged, but more of the line must be searched, given a particular mass range prediction, as shape will shift this further along the line. However, since multiple scenarios overlap, several can be effectively searched at the same time.

3.4 Monte Carlo studies of fall line variations and scatter

To combine all these factors, and generate some understanding of the associated uncertainties that predictions would generate in the case of Murrili, we have carried out Monte Carlo simulations of darkflight descents covering ranges

- with mass in range of 1.5-2.3 kg, based on pre-recovery predictions from (Sansom et al. 2020)
- with a density 3500 kg/m³
- first with no atmospheric winds, then allowing variation of up to +/-5 % in wind magnitude and direction for a wind profile, using the data based on the 00:00 snapshot, chosen for reasons discussed in section 3.2. The 5% uncertainty is derived from the deviation of the profile variations seen in Figure 5.
- meteorite shape can vary from spherical to a rounded brick shape—defined as 2.5 x 1.5 x 1 brick dimensions with corners smoothed off, using the rationale and estimates of (Zhdan et al. 2007), with the highest drag direction of the brick orientated in the direction of travel. For wind effects acting transverse to the orientated brick, we use the drag coefficients from (Zhdan et al. 2007) for a cube shaped object. (For non-spherical objects in supersonic regimes, the object usually settles into an orientation with the maximum cross section across the trajectory, giving the maximum drag coefficient, as detailed in (Turchak and Gritsevich 2014) and references therein.)

These Montecarlo ground positions are then displayed as scatter maps in Figure 8.



281

282

283

284

285

Figure 8 (a) Monte Carlo results of 0.5-2kg chondritic meteorite, 1000 runs, allowing initial shape to vary from sphere to rounded brick (b) same but with wind variation of 5% allowed in direction and magnitude of the 00:00 snapshot based wind profile provided by WRF. The simulations also allow variation in the initial vector from end of bright flight triangulation, using the uncertainties in Table 2.

The ground scatter plots are very roughly the same location, although with greater scatter as wind due to wind. In overall dimensions, the scatter distributions are about 200 m orthogonal to the fall line, indicating a reasonable distance to search from the fall lines, and rough length along fall line of both scatters is 400 m, giving each a searchable area of about 0.2 km².

3.5 Fall line prediction compared to meteorite recovered position

The previous sections describe the analysis that can be done before meteorite recovery, using shape approximations and wind model predictions. We now consider after the meteorite recovery, when the actual shape, mass, density are known, and a newer version of the WRF is available. Despite the high quality of triangulation and the low end point of the bright flight, the fall position was ~40 m away from the preferred line prediction, and ~100 m along the line from a sphere-based prediction. This would at first glance appear excellent from a practical searching point of view, but for a less favourable fall with a higher end point this offset would be proportionally larger. For a shallower entry angle, fall line uncertainties also increase due to greater horizontal travel at high velocity immediately after the end of bright flight, where any unknowns in the drag coefficient and shape contribute greatly. One should then investigate possible causes for this orthogonal offset: Since many factors are constrained by the properties of the meteorite, one is essentially left with issues of wind models accuracy, a non-ideal shape, or modelling issues such as choice of drag coefficient. The preceding analysis has focused on the data available prior to recovery, but for the following figures using post recovery data, fall lines are plotted use a later recalculation of the wind models, using WRF v3.9.1, which has shifted the fall line predictions slightly, by about 100 m to the south.

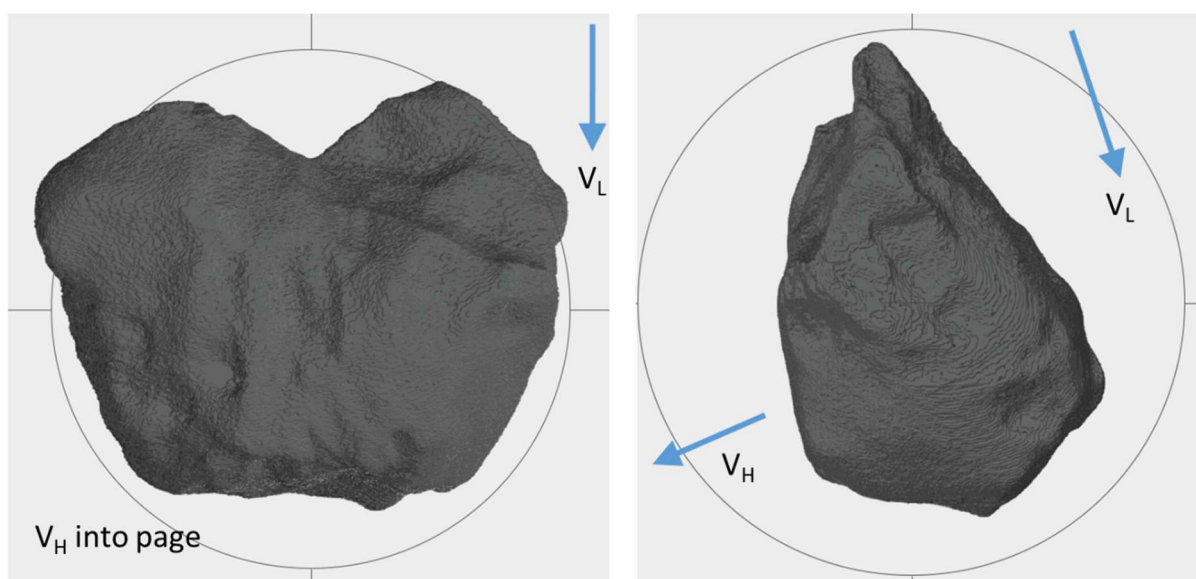


Figure 9 Murrili meteorite dimensions and shape. Compared to a sphere, the rock is flattened and heart-shaped, but almost teardrop from the side view

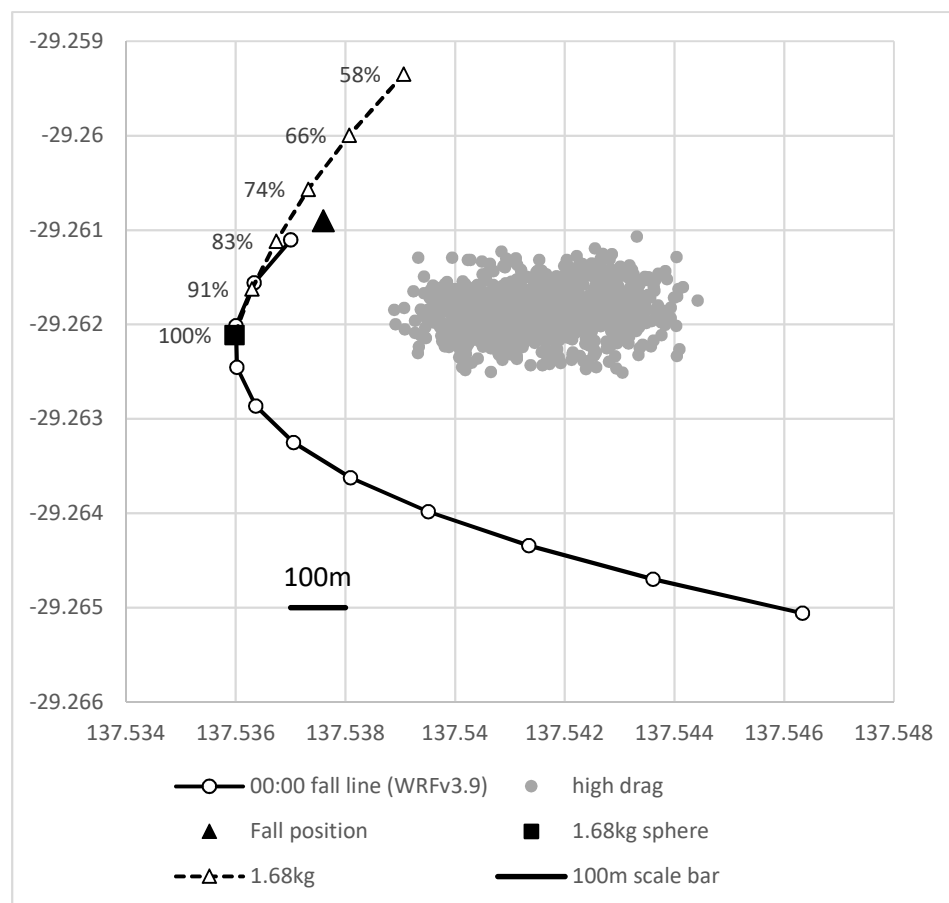
311

312 The Murrili meteorite is shown in Figure 9. Its extents in (a) are approximately 130mm x 90mm,
313 while the thickness in (b) is 70 mm. We round to the nearest 5 mm due to fine detail irregular
314 variations in surface features. The meteorite volume (obtained from a CT scan) is
315 474,731 mm³, giving an equivalent sphere radius of 48 mm (volumetric radius). Alternatively,
316 the meteorite surface area is 40,299 mm², giving a sphericity of 0.71 or 0.73 depending on the
317 definition used; surface area of an equivalent volume sphere over surface area of meteorite is
318 28,952/40,299 giving 0.71 (Pettijohn 1975), or alternatively equivalent volume sphere
319 diameter over diameter of circumscribing sphere is 96 mm/130 mm giving 0.73 (Wadell 1935).
320 As part of the meteorite description studies prior to official classification, the meteorite was
321 visually inspected, and we have reviewed the 3D CT scan data to investigate any fusion crust
322 features that might hint at orientation or even changes in flow regime during descent – there
323 are some possible flow lines, but they are very faint and quite subjective, and not completely
324 compelling. Unfortunately, the meteorite fell into a wet salt lake in the Australian summer, and
325 so was buried for about a month in warm saltwater mud before recovery. The extensive
326 weathering appears to have removed a lot of fine detail, preventing any firm conclusions about
327 orientation. We have also reviewed the details of the impact site for insight into orientation, via
328 images of the impact itself, and consideration of the impact velocity. The impact appears
329 roughly circular in form (Sansom et al. 2020), although the salt lake crust may break unevenly.
330 (Sansom et al. 2020) additionally states that meteorite was buried 42 cm into the mud.
331 However, the lack of knowledge of the properties of the ground, as needed for the appropriate
332 projectile depth penetration equations (Young 1967, 1997) can generate a wide range of
333 velocities, providing little guidance on reconstructing the impact velocity.

334 One can attempt to correct the spherical drag coefficient with some factor based on the known
335 shape of the recovered meteorite. For non-spherical bodies, this problem has been studied in
336 the context of dust settling rates, often in relation to industrial processes or environmental
337 studies. See for example (Connolly et al. 2020) and references therein, or (Kleinstreuer and
338 Feng 2013) for a review from a biomedical context. For settling rate studies, the Corey Shape
339 Factor, CSF, ($d_{\min}/\sqrt{(d_{\max}*d_{\text{med}})}$ where d is diameter, (Corey 1949), is the most commonly used
340 approximation and provides the most data for correlations between publications. For Murrili
341 this evaluates to 0.64. However, one must exercise caution with using CSF outside of settling
342 studies – a CSF of 1.0 describes a sphere, a cube or several other regular solids, which all
343 have different drag coefficients.

344 Free fall drag coefficient has also been derived as a function of sphericity from empirical and
345 theoretical studies ((Haider and Levenspiel 1989) and references therein). Within the DFN
346 general darkflight code implementation it is possible to explicitly specify sphericity (Table 1,
347 forcing the use of Haider and Levenspiel, equation 11), overriding the default calculations for
24

a sphere. (Hölzer and Sommerfeld 2008) extend this formulation to include projectile orientation, by treating crosswise and longitudinal sphericity separately. To investigate and compare this, we have implemented their equation 9, and then calculated Monte Carlo darkflight simulations with Murrili falling teardrop-orientated (low drag), and then flat-orientated (high drag). We indicate these directions of travel shown arrows V_L and V_H in Figure 9). In Figure 10 we show the results of these Monte Carlo simulations. We exactly specify the meteorite mass and density, but permit initial vector variation and 5% wind uncertainties. For reference to previous figures we also display the 00:00 fall line (based on a spherical drag coefficient, but with the later WRF v3.9 wind model) and meteorite recovery location.



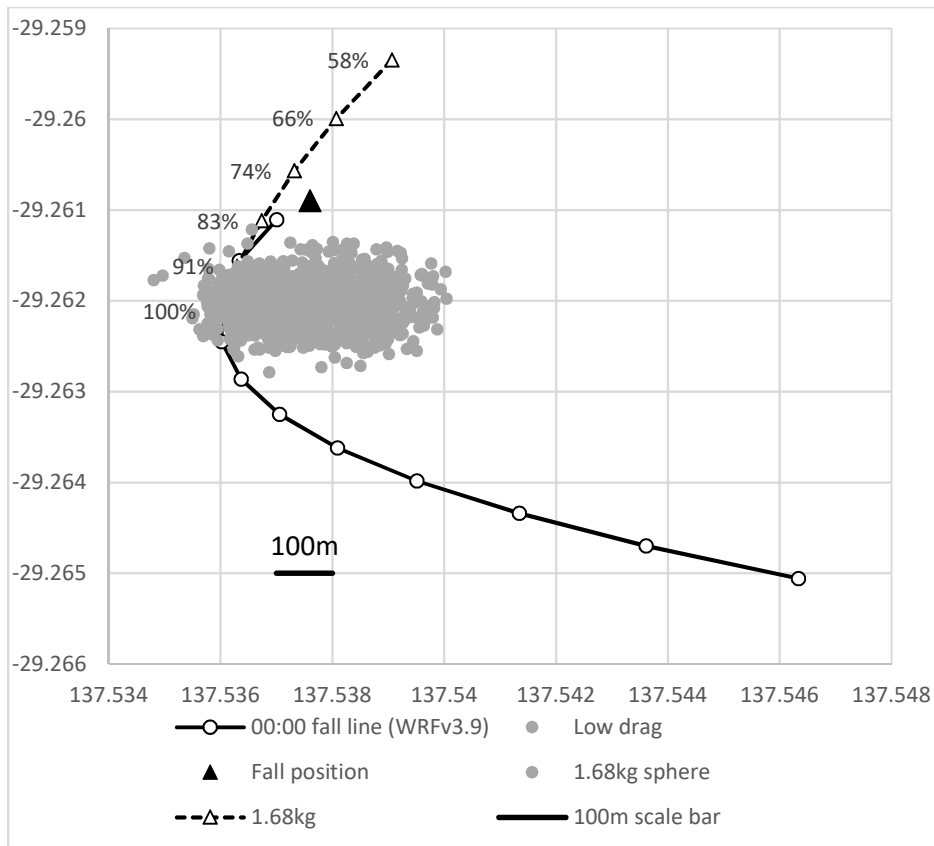


Figure 10 Monte Carlo

simulations of Murrili (fixed at 1.68 kg, 3500 kg/m³) falling at different orientations. (a) showing the scatter for falling in a high drag orientation (Horizontal orientation in Figure 9), (b) in a low drag orientation (Vertical in Figure 9), as indicated by fall direction arrows in Figure 9. Percent line is described in the text.

Considering the scatter points in Figure 10, we can see that fall orientation clearly will have an effect. (a) shows that the high drag orientated simulations are somewhat offset from the isotropic drag fall line, and from the recovery position (triangular marker). Figure 10(b) shows the vertically orientated (falling in a teardrop orientation, with lowest possible drag coefficient in direction of travel) scatter as a closer match, intersecting the isotropic fall line but not intersecting the recovery position

The actual position of the impact is close to the isotropic fall line, but ~400 m along the line from the 1.68 kg prediction (black square marker) which corresponds to an anomalously large mass (>5 kg). By beginning with a spherical isotropic object, and keeping mass fixed at 1.68 kg, but reducing the drag coefficient in all directions (so using Table 2, but with a scalar reduction in forces as labelled), we generate the dashed/triangle line that is oblique to the isotropic fall line. This line also doesn't pass precisely through the impact point, and the closest approach is when drag reduced by about 75% (so a scalar factor of 0.75) compared to a sphere. The closest approach distance is 44 m.

The relative lack of cross-track offset between the impact point and the isotropic sphere fall line may result from the wind modelling not matching reality: In general isotropic drag changes from shape, density, or mass variations act to effectively shift objects either along the fall line or very close to it, rather than away from the line (The sphere and brick fall lines in Figure 2 are essentially the same line extended). Note also how the isotropic sub-sphere line in Figure 10 is sub-parallel to the sphere line, not at some arbitrary angle. The recovered meteorite does not precisely align with either of the isotropic lines; this offset is either from small amount of non-spherical drag (aerodynamic shape effects such as angle of attack or lift), or most likely from just basic inaccuracies in the wind model.

Comparing the Monte Carlo point clouds for the two orientations, the two orientated point clouds do not bracket the spherical fall line, as one might initially imagine, as the influence of sphericity means that sideways wind effects are decoupled from vertical velocity. The difference between the centres of the clouds is shifted East and slightly South (from high to low drag), which corresponds to the general wind orientations of approximately 270-300° in Figure 5b. These point clouds can be thought of as representing extremes on a spectrum of orientations, and some intermediate orientation value would lie in between these clouds. However, no intermediate value would pass through the actual impact site, which hints that perhaps the modelled wind data has some inaccuracy, most likely due to lack of real supporting measurements.

In both cases the diameter and scatter of the orientated Monte Carlo point clouds are smaller than the isotropic sphere scatter as seen in Figure 8b: We hypothesise that the sphere has a unique combination of properties of wind influence and vertical fall velocity; so, the low drag orientation is most influenced by the horizontal winds, but vertically falls a lot quicker, with less time for the wind influence to act, and vice versa for the high drag orientation.

In Figure 10a, the difference in position between the high drag orientated point cloud and the isotropic sphere fall line (and the impact point) appears relatively large, compared to the low drag cloud. This appears somewhat counterintuitive, as one might expect the low drag down orientation (which has a high drag sideways) to have bigger shift from the sphere line. This shift must result from the higher drag giving a longer dwell time (slower fall velocity), giving the winds greater influence.

Although the low drag (vertical orientation) Monte Carlo simulation appear closer than the high drag simulation to the recovery point, neither orientation overlaps this point. In Figure 8b, the Monte Carlo simulation of an isotropic sphere does however overlap the recovery point: The wind model can be compatible with an isotropic object, but not an orientated fall, although an irregular shape with complex tumbling may effectively cancel out any orientation effects.

So we result in several possible scenarios to reconcile the data with the modelling: wind models approximately correct, but with an isotropic shape having an anomalously low drag

coefficient, or an isotropic shape where winds are lower or less influential than expected (or a reduced drag coefficient). Finally, an orientated shape falling seems less likely, as the wind models would have to be substantially incorrect, which is not supported by other recoveries, both DFN and other fireball networks around the world.

These possibilities are not exclusive, as the Australian outback real wind observations are sparse. A change of orientation during flight, and even rotation could not be ruled out, and might have the effect of damping the effects of orientation. Even in the low drag scenario, strong horizontal winds would have the effect of altering the angle of attack of the falling rock, which will have aerodynamic effects. From this single event it is difficult to separate these possibilities, but analysis of further falls should show which is the appropriate formulation to use in future predictions.

These scatter plots, and also the shape dependence of points along the fall line in Figure 7 illustrate the both the need to search widely along an ideal fall line prediction, and the dominance of shape in darkflight modelling. Any shape characteristics available from bright flight behaviour will be most helpful, but detailed shape is unlikely to be known. The reasonable match between basic predictions and the recovered fall position, would tend to indicate that the wind model chosen in this case is probably sufficiently accurate (i.e. not the major source of uncertainty), and that also that geometric errors in triangulation are relatively minor. Assuming a specific orientation during darkflight does not provide best fit, but simple assumptions can be helpful in planning searching. In contrast to the spherical or lower drag coefficient here demonstrated, another DFN recovery, the Dingle Dell meteorite, landed 105 m from fall line, but at a point along the line that corresponds to a cylindrical mass, with a drag coefficient significantly greater than spherical. ((Dewillepoix et al. 2018), their figure 10). However, we must note that Dingle Dell suffered from several complicating issues: the recovered meteorite has an angular broken surface, implying fragmentation, which was supported by the light curve; the entry angle was also shallow, and end point slightly higher (19.1 km). However, in both Murrili and Dingle Dell cases the offset between fall lines and recoveries, and the position along the line are relatively manageable a searching point of view.

4 CONCLUSIONS

For fireball camera networks, focussed towards meteorite recovery, the calculation of the darkflight trajectory after luminous observations is a critical step to sample recovery. This step is very difficult to test, due to the lack of observations during descent, with only the recovery (or not) of the meteorite providing a data point. The principles of darkflight calculation are simple, based on a classical aerodynamic drag equation, but the calculation hides subtleties, particularly in the formulation of aerodynamic properties. We describe the details and

approach taken to this problem by the Desert Fireball Network. The simplest output from a darkflight calculation is typically a fall line, showing impact positions for a known range of hypothetical masses. From consideration of these lines, and the effects of parameters, we find that the choice of meteorite shape is more important than density or mass choice, in terms of variation in ground position. These constraints in turn influence the ground searching strategy. We illustrate this with a case study of the Murrili meteorite fall, recovered from Lake Eyre-Kati Thanda in 2015. Murrili is ideal case for darkflight study, as the optical observations and triangulation data were exceptionally good, with multiple DFN observatories relatively close by giving a range of viewpoints. Additionally, the meteor trajectory was steep, and the final height at the end of the luminous phase was at a relatively low altitude of 18 km, so the darkflight was relatively short, compared to many meteorite falls. However, winds were quite strong at this location, especially around the 15 km levels, so the darkflight fall line was perturbed significantly. Given the known location of the meteorite impact point and the known shape, we investigate whether the meteorite had an orientation during fall, and find that although the final position can be matched using an orientation with the lowest drag coefficient in the direction of travel rather than the highest, the fall position is best matched by assuming a either a spherical shape and drag characteristics, or a reduced drag sphere, where one assumes spherical properties, and then artificially reduces the influence of atmospheric interactions (to about 75% in this case). A simple isotropic approach like this may provide a way forward to investigate weakly constrained shapes for observed falls; other falls seen by the DFN are also well matched with an isotropic shape, but not necessarily a pure sphere. We note from this that Murrili although is close to an ideal case for darkflight modelling, it was still necessary to consider in detail the overall shape of the meteorite and the detailed atmospheric properties in order to get a good agreement between predicted and observed fall positions. Further work would benefit greatly from detailed published data concerning the shape of recovered meteorites, in combination with precise details of the end of luminous trajectory, so that aerodynamically realistic drag coefficients could be estimated, and compared to the recovery positions.

5 ACKNOWLEDGEMENTS

We thank the Arabana people, the traditional custodians of Kati Thanda, for their support during meteorite searching. This work is funded by the Australian Research as part of the Australian Discovery Project scheme (DP170102529). This work was supported by resources provided by the Pawsey Supercomputing Centre with funding from the Australian Government and the Government of Western Australia. We thank the Australian Wildlife Conservancy for

their support in maintaining the Kalamurina DFN camera. We thanks two anonymous reviewers for the comments which greatly improved this paper.

6 REFERENCES

- Astropy Collaboration, Price-Whelan AM, Sipőcz BM, et al (2018) The Astropy Project: Building an Open-science Project and Status of the v2.0 Core Package. *Astron J* 156:123. <https://doi.org/10.3847/1538-3881/aabc4f>
- Borovička J (1990) The comparison of two methods of determining meteor trajectories from photographs. *Bull Astron Inst Czechoslov* 41:391–396
- Borovička J, Kalenda P (2003) The Morávka meteorite fall: 4. Meteoroid dynamics and fragmentation in the atmosphere. *Meteorit Planet Sci* 38:1023–1043. <https://doi.org/10.1111/j.1945-5100.2003.tb00296.x>
- Carter RTJ (2011) Constraining the Drag Coefficients of Meteors in Dark Flight
- Ceplecha Z (1961) Multiple fall of Příbram meteorites photographed. *Bull Ast Inst Cz* 2:21
- Ceplecha Z (1987) Geometric, dynamic, orbital and photometric data on meteoroids from photographic fireball networks. *Bull Astron Inst Czechoslov* 38:222–234
- Ceplecha Z, Borovička J, Elford WG, et al (1998) Meteor phenomena and bodies. *Space Sci Rev* 84:327–471
- Ceplecha Z, Borovička J, Spurný P (2000) Dynamical behavior of meteoroids in the atmosphere derived from very precise photographic records. *Astron Astrophys* 357:1115–1122
- Colas F, Zanda B, Bouley S, et al (2014) The FRIPON and Vigie-Ciel networks. pp 34–38
- Connolly BJ, Loth E, Smith CF (2020) Shape and drag of irregular angular particles and test dust. *Powder Technol* 363:275–285. <https://doi.org/10.1016/j.powtec.2019.12.045>
- Corey AT (1949) Influence of shape on the fall velocity of sand grains. Colorado State University
- Devillepoix HAR, Sansom EK, Bland PA, et al (2018) The Dingle Dell meteorite: A Halloween treat from the Main Belt. *Meteorit Planet Sci* 53:2212–2227. <https://doi.org/10.1111/maps.13142>
- Flynn GJ (2005) Physical Properties of Meteorites and Interplanetary Dust Particles: Clues to the Properties of the Meteors and their Parent Bodies. In: Hawkes R, Mann I, Brown P (eds) *Modern Meteor Science An Interdisciplinary View*. Springer Netherlands, pp 361–374
- Folinsbee RE, Bayrock LA (1961) The Bruderheim Meteorite-Fall and Recovery. *J R Astron Soc Can* 55:218
- Fries M, Fries J (2010) Doppler weather radar as a meteorite recovery tool. *Meteorit Planet Sci* 45:1476–1487. <https://doi.org/10.1111/j.1945-5100.2010.01115.x>
- Gritsevich M, Lyytinen E, Moilanen J, et al (2014) First meteorite recovery based on observations by the Finnish Fireball Network
- Gritsevich MI (2007) Approximation of the observed motion of bolides by the analytical solution of the equations of meteor physics. *Sol Syst Res* 41:509–514. <https://doi.org/10.1134/S003809460706007X>
- Haider A, Levenspiel O (1989) Drag coefficient and terminal velocity of spherical and nonspherical particles. *Powder Technol* 58:63–70. [https://doi.org/10.1016/0032-5910\(89\)80008-7](https://doi.org/10.1016/0032-5910(89)80008-7)
- Halliday I, Blackwell AT, Griffin AA (1978) The Innisfree meteorite and the Canadian Camera Network. *J R Ast Soc Can* 72:15–39
- Hölzer A, Sommerfeld M (2008) New simple correlation formula for the drag coefficient of non-spherical particles. *Powder Technol* 184:361–365. <https://doi.org/10.1016/j.powtec.2007.08.021>
- Howie RM, Paxman J, Bland PA, et al (2017) How to build a continental scale fireball camera network. *Exp Astron* 43:237–266. <https://doi.org/10.1007/s10686-017-9532-7>
- Jacchia LG, Whipple FL (1956) The Harvard photographic meteor programme. *Vistas Astron* 2:982–994. [https://doi.org/10.1016/0083-6656\(56\)90021-6](https://doi.org/10.1016/0083-6656(56)90021-6)
- Jenniskens P, Fries MD, Yin Q-Z, et al (2012) Radar-Enabled Recovery of the Sutter's Mill Meteorite, a Carbonaceous Chondrite Regolith Breccia. *Science* 338:1583–1587. <https://doi.org/10.1126/science.1227163>
- Jones E, Oliphant T, Peterson P (2001) SciPy: Open source scientific tools for Python
- Khanukaeva DYU (2003) On the Coefficients in Meteor Physics Equations. *AIP Conf Proc* 663:726–734. <https://doi.org/10.1063/1.1581615>

- Kleinstreuer C, Feng Y (2013) Computational Analysis of Non-Spherical Particle Transport and Deposition in Shear Flow With Application to Lung Aerosol Dynamics—A Review. *J Biomech Eng* 135:. <https://doi.org/10.1115/1.4023236>
- Masson DJ, Morris DN, Bloxom DE (1960) Measurements of sphere drag from hypersonic continuum to free-molecule flow. RAND Corporation
- McCrosky RE, Posen A, Schwartz G, Shao C-Y (1971) Lost City meteorite—Its recovery and a comparison with other fireballs. *J Geophys Res* 76:4090–4108. <https://doi.org/10.1029/JB076i017p04090>
- Miller DG, Bailey AB (1979) Sphere drag at Mach numbers from 0.3 to 2.0 at Reynolds numbers approaching 10^7 . *J Fluid Mech* 93:449–464. <https://doi.org/10.1017/S00222112079002597>
- Passey QR, Melosh HJ (1980) Effects of atmospheric breakup on crater field formation. *Icarus* 42:211–233. [https://doi.org/10.1016/0019-1035\(80\)90072-X](https://doi.org/10.1016/0019-1035(80)90072-X)
- Pecina P, Ceplecha Z (1983) New aspects in single-body meteor physics. *Bull Astron Inst Czechoslov* 34:102–121
- Pettijohn FJ (1975) *Sedimentary Rocks*. Harper and Row, New York
- ReVelle DO (2005) Recent Advances in Bolide Entry Modeling: A Bolide Potpourri*. *Earth Moon Planets* 97:1–35. <https://doi.org/10.1007/s11038-005-2876-4>
- Revelle DO (2002) Fireball dynamics, energetics, ablation, luminosity and fragmentation modeling. pp 127–136
- Sansom EK, Bland P, Paxman J, Towner M (2015) A novel approach to fireball modeling: The observable and the calculated. *Meteorit Planet Sci* 50:1423–1435. <https://doi.org/10.1111/maps.12478>
- Sansom EK, Bland PA, Towner MC, et al (2020) Murrili meteorite's fall and recovery from Kati Thanda. *Meteorit Planet Sci* 55:2157–2168. <https://doi.org/10.1111/maps.13566>
- Sansom EK, Gritsevich M, Devillepoix HAR, et al (2019) Determining Fireball Fates Using the alpha–beta Criterion. *Astrophys J* 885:115. <https://doi.org/10.3847/1538-4357/ab4516>
- Sansom EK, Rutten MG, Bland PA (2017) Analyzing Meteoroid Flights Using Particle Filters. *Astron J* 153:87. <https://doi.org/10.3847/1538-3881/153/2/87>
- Skamarock C, Klemp B, Dudhia J, et al (2019) A Description of the Advanced Research WRF Model Version 4. <https://doi.org/10.5065/1dfh-6p97>
- Skamarock WC, Klemp JB, Dudhia J, et al (2008) A Description of the Advanced Research WRF Version 3. National Center for Atmospheric Research
- Spurný P, Bland PA, Borovicka J, et al (2012) The Mason Gully Meteorite Fall in SW Australia: Fireball Trajectory, Luminosity, Dynamics, Orbit and Impact Position from Photographic Records. 1667:6369
- Spurný P, Bland PA, Shrbený L, et al (2012) The Bunburra Rockhole meteorite fall in SW Australia: fireball trajectory, luminosity, dynamics, orbit, and impact position from photographic and photoelectric records. *Meteorit Planet Sci* 47:163–185. <https://doi.org/10.1111/j.1945-5100.2011.01321.x>
- Spurný P, Borovička J, Shrbený L (2006) Automation of the Czech part of the European fireball network: equipment, methods and first results. *Proc Int Astron Union* 2:121–130. <https://doi.org/10.1017/S1743921307003146>
- Turchak LI, Gritsevich MI (2014) Meteoroids Interaction With The Earth Atmosphere. *J Theor Appl Mech* 44:15–28. <https://doi.org/10.2478/jtam-2014-0020>
- Vinnikov VV, Gritsevich MI, Turchak LI (2016) Mathematical model for estimation of meteoroid dark flight trajectory. *AIP Conf Proc* 1773:110016. <https://doi.org/10.1063/1.4965020>
- Wadell H (1935) Volume, Shape, and Roundness of Quartz Particles. *J Geol* 43:250–280. <https://doi.org/10.1086/624298>
- Young CW (1967) Development Of Empirical Equations For Predicting Depth Of An Earth-Penetrating Projectile. Sandia Corp., Albuquerque, N. Mex.
- Young CW (1997) Penetration equations. Sandia National Lab. (SNL-NM), Albuquerque, NM (United States)
- Zhdan IA, Stulov VP, Stulov PV, Turchak LI (2007) Drag coefficients for bodies of meteorite-like shapes. *Sol Syst Res* 41:505–508. <https://doi.org/10.1134/S0038094607060068>